Aminoacid substitutions in the glycine zipper affect the conformational stability of amyloid beta fibrils

(Article begins on next page)

14 June 2021

Manuscript

Aminoacid Substitutions in the Glycine Zipper Affects the Conformational Stability of Amyloid Beta Fibrils

Gianvito Grasso[1*], Luigi Leanza[2], Umberto Morbiducci[2], Andrea Danani[1], and Marco A. Deriu[2]

[1]*Dalle Molle Institute for Artificial Intelligence (IDSIA), University of Applied Sciences of Southern Switzerland (SUPSI), University of Italian Switzerland (USI), Centro Galleria 2, Manno, CH-6928, Switzerland.*
[2]*Department of Mechanical and Aerospace Engineering (DIMEAS), Politecnico di Torino, Corso Duca degli Abruzzi 24, IT-10128, Torino, Italy.*

*Corresponding author
Gianvito GRASSO, PhD
Istituto Dalle Molle di studi sull'Intelligenza Artificiale (IDSIA),
Scuola universitaria professionale della Svizzera italiana (SUPSI)
Centro Galleria 2, Manno, CH-6928, Switzerland
marco.deriu@idsia.ch
phone: +41 586666568
[*]gianvito.grasso@idsia.ch

Abstract

The aggregation of amyloid-beta 42 (Aβ_{42}) peptides is associated with the pathogenesis of Alzheimer's Disease. Within the hydrophobic core of the Aβ sequence, there is a repeated GxxxG motif involving essential residues for assuring stability and promoting the process of fibril formation, called *glycine zipper*. Mutations in this motif lead to a completely different oligomerization pathway and rate of fibril formation. In this work, we have tested G33L and G37L residue substitutions by Molecular Dynamics simulations. We found that both protein mutations, and in particular the G33L replacement, leads to remarkable changes in the fibril conformational stability. These results suggest the disruption of the glycine zipper as a possible strategy to reduce the aggregation propensity of Aβ_{42}. On the basis of our data, further investigations may consider this key region as a binding site for small molecules with the final aim of reducing the stability of the Aβ fibrils.

Introduction

Alzheimer's disease (AD) is the most common presenile neurodegenerative disease. Three main hypotheses have been proposed about the AD etiology(Huet & Derreumaux, 2006) : Tau hypothesis(Bartus, 2000), Cholinergic hypothesis(Bartus, 2000) and Amyloid cascade hypothesis(Hardy & Selkoe, 2002). Amyloid hypothesis is among the most widely accepted models(Ngo, Nguyen, Nguyen, & Vu, 2017) and supported by preclinical and clinical data(Hardy & Selkoe, 2002; Selkoe & Hardy, 2016). Amyloid Beta (Aβ) peptide derives from the transmembrane amyloid precursor protein (APP), via endoproteolytic cleavage by β- and γ- secretase(Cummings, 2004). In detail, the proteolytic cleavage of APP produces Aβ peptides of different amino acid length. Senile plaques are primarily composed of $A\beta_{40}$, the most abundant, and $A\beta_{42}$, the most toxic(Gravina et al., 1995; Lee et al., 2017; Querfurth & LaFerla, 2010; Roher et al., 1993).

On the basis of solid-state NMR restraints, different structural models of $A\beta_{40}$ and $A\beta_{42}$ fibrils have been proposed(Colvin et al., 2016b; Lu et al., 2013; Lührs et al., 2005; Paravastu, Leapman, Yau, & Tycko, 2008; Qiang, Yau, Luo, Mattson, & Tycko, 2012; Schütz et al., 2015; Wälti et al., 2016; Xiao et al., 2015), since Aβ fibrils are characterized by structural polymorphism at molecular level(Fändrich, Meinhardt, & Grigorieff, n.d.). In detail, $A\beta_{40}$ can adopt only a U-shaped structure(Xi, Wang, Abbott, & Hansmann, 2016) characterized by β-strands (Y10-D23, A30-G38), connected by a beta-sheet (G25-G29) (Petkova et al., 2002) and stabilized by interchain hydrogen bonds and salt-bridges (D23-K28). The $A\beta_{42}$ can arrange also in a S-shaped structure(Xi et al., 2016). The S-shaped $A\beta_{42}$ species consist of three β-strands: β_1 strand is made of residues V12-V18, β_2 strand of residues V24-G33 and β_3 strand of residues V36-V40, connected by coil and turn regions and stabilized by intermolecular hydrogen bonds and salt-bridges. Recent studies(Acosta, Vega, Basurto, Morales, & Rosales Hernández, 2018; Gianvito Grasso et al., 2019, 2018) demonstrated that the S-shaped $A\beta_{42}$ is the most stable and compact specie if compared with the U-shaped $A\beta_{42}$. Within this context, we have recently demonstrated how the S-shaped $A\beta_{42}$ is characterized by a greater

conformational (Gianvito Grasso et al., 2018) and mechanical (Gianvito Grasso et al., 2019) stability.

Amyloid fibrils have been studied in a huge number of both experimental and computational works, given the intimate relationship between conformational structure and disease onset. Mutations of protein residues can modify the physico-chemistry of the $A\beta_{42}$ and alter the toxicity of the resulting fibrils. In particular, an experimental study of the fibrillization kinetics with scanning mutagenesis identified six residues to be essential for the formation of $A\beta_{42}$ fibrils: H14, E22, D23, G33, G37 and G38(Hsu, Park, & Guo, 2018).

It is worth mentioning that three of the previously-mentioned residues are glycine. Experimental studies demonstrated that glycine stabilizes the packing of β-sheets in the formation of amyloid fibrils(Liu et al., 2005). This evidence can explain the importance of G33, G37 and G38 in aggregation process. G33 and G37 residue are also involved in a GxxxG motif, called glycine zipper(Kim et al., 2005). This motif includes four glycine residues within the hydrophobic region (G25, G29, G33 and G37) and this motif facilitates the conversion of α-helices and random coils to β-sheet and thus promote the fibril formation(Harmeier et al., 2009; Liu et al., 2005; Munter et al., 2007). Replacing G33 and G37 with leucine destabilizes the fibril structure by disrupting the glycine-zipper packing interface(Harmeier et al., 2009; Kim et al., 2005; Sato et al., 2006). Moreover, in vivo and in vitro studies(Fonte et al., 2011; Harmeier et al., 2009; Hung et al., 2008) showed a reduced aggregation propensity in Aβ_{42} by G33 and G37 substitution with alanine, isoleucine or leucine. A computational analysis(Harmeier et al., 2009) illustrated that conformational changes of Aβ_{42} G33 variants are induced by increased hydrophobicity. Chiti et al(Chiti, Stefani, Taddei, Ramponi, & Dobson, 2003) has previously demonstrated the correlation between the aggregation rate of peptides and changes in hydrophobicity. However, the precise destabilization mechanism of G-to-L substitutions remain still unclear.

Computational studies, especially when associated with experimental evidences, can be a powerful tool able to yield an insight into molecular leve(Bidone, Kim, Deriu, Morbiducci, & Kamm, 2015; Soncini et al., 2007) and to investigate how the above-mentioned mutations affect mechanisms of

aggregation, oligomerization pathways(Deriu et al., 2016; G Grasso et al., 2018) and rate of fibril formation.

The present study focuses on investigating the conformational dynamics of Aβ_{42} in presence of two glycine-to-leucine substitutions, G33L and G37L. The previously mentioned mutations were studied by considering two different S-shaped $A\beta_{11-42}$ fibril models (Colvin et al., 2016a; Xiao et al., 2015) in order to take into account the well-known polymorphic nature of Aβ_{42} at molecular level. Our MD results suggest that both mutations, and in particular the G33L substitution, dramatically reduces the stability of Aβ_{11-42}.

Material and methods

Computational Setup

Two different 9-mer models of S-shaped $A\beta_{11-42}$specie were studied: one extracted from PDB ID: 2MXU(Xiao et al., 2015) and one from PDB ID: 5KK3(Colvin et al., 2016a). G33L and G37L mutants were obtained by using CHIMERA(Pettersen et al., 2004) mutation tool, from the corresponding wild-type specie of 2MXU and 5KK3 (Supplementary Figure S1). All the models were solvated in an 8 nm cubic box and neutralized by counterions. Each system consisted of about 50,000 particles. The CHARMM36 force field(Huang et al., 2016) was used to define protein topologies and the TIP3P (Jorgensen, Chandrasekhar, Madura, Impey, & Klein, 1983) model was used for the explicit solvent. GROMACS 5.1.4(Abraham et al., 2015) version was employed for simulations. Steepest descent algorithm(Fletcher & Powell, 1963) was utilized to minimize the system. Then, a 50 ps simulation in NVT ensemble was conducted, by applying the V-rescale algorithm(Bussi, Donadio, & Parrinello, 2007) to keep temperature at 300 K and time constant of 0.1 ps. In order to increase the statistic, five replicas for each $A\beta_{11-42}$model were generated. A 50 ps simulation in a NPT ensemble for each replica was carried out. Weak coupling methods(Berendsen, Postma, Van Gunsteren, DiNola, & Haak, 1984; Bussi et al., 2007) were used for pressure and temperature control. Finally, for each replica 100 ns long MD were simulated coupling the system by Nose-Hoover(Evans & Holian, 1985) and Parrinello-Rahman(Berendsen et al., 1984), for temperature and pressure respectively. The LINCS algorithm(Hess, Bekker,

Berendsen, & Fraaije, 1997) was used to constrain the length of h-bonds. Electrostatics was treated by PME algorithm(Darden, York, & Pedersen, 1993). Trajectories were extracted every 50 ps of simulation and the Visual Molecular Dynamics (VMD) package(Humphrey, Dalke, & Schulten, 1996) was employed to provide the visual inspection of the simulated systems. The secondary structures were obtained by STRIDE (Heinig & Frishman, 2004). The structural stability of the fibril models was evaluated by computing an order parameter (*ordP*) as already done in a recent study (Gianvito Grasso et al., 2018). The *ordP* was calculated as reported below:

$$ordP = \frac{1}{N} \sum_{r=11}^{42} \frac{\langle v_r, x \rangle}{\|v_r\| \cdot \|x\|} = \frac{1}{N} \sum_{r=11}^{42} \cos \alpha$$

Where v_r is the vector joining C_α-atom of each residue *r* of chain A with the corresponding C_α-atom of the same residue of chain I and *x* is the fibril axis. If ordP assumes values close to 1, the chains maintain an alignment to the initial structure; if the values of ordP are lower than 1, the overall structural order decreases. Further details about the ordP calculation are reported in Supporting Information S2.

Results

Results reported in the following refer to S-shaped $A\beta_{11-42}$(2MXU, and 5KK3) in wild type and mutated forms (G33L and G37L). Unless otherwise specified, equilibrium properties have been calculated on the last 20 ns of all trajectories, taken as conformational ensemble. The Wild Type simulations of 2MXU and 5KK3 models will be indicated as 2MXU-WT and 5KK3-WT, respectively.

The protein fluctuations were evaluated by Root Mean Square Fluctuation (RMSF) analysis and it is shown in Figure 1. RMSF values show how N-terminal tail is the most flexible region. It is worth mentioning that the 5KK3-WT model shows an increased value of RMSF in the region E11-K16 if compared with 2MXU-WT model.

The G33L mutation leads to an overall increase in fluctuation values in both models, indicating the destabilization of the fibril conformation in presence of protein mutations. In detail, G33L mutation strongly affects the flexibility of the central core (E22-K28) and C-terminal regions (Figure 1).

The effect of G37L mutation is less severe. In the 2MXU model, the substitution affects the C-terminal region only. On the other hands, the 5KK3 model shows almost identical values of flexibility along the chain, when compared with WT specie, except for the mutated site ($RMSF_{37}[5KK3G37L]=0,117\pm0,017\,nm$, $RMSF_{37}[5KK3WT]=0,073\pm0,010\,nm$).
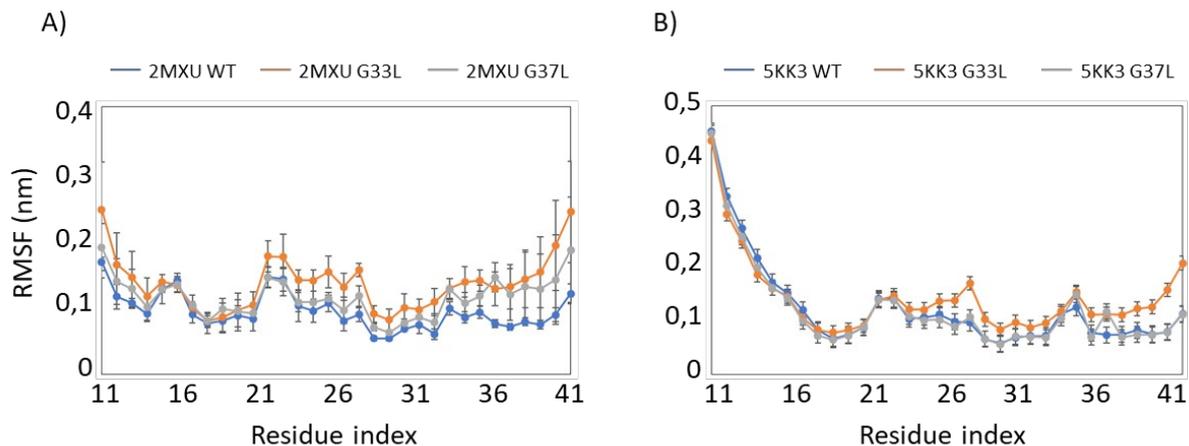
A)

B)

Figure 1:RMSF of structures as a function of residue and relative standard deviation, calculated as the average over the last 20 ns of MD trajectory for each simulation.

As widely demonstrated in scientific literature(Kung, Cornilescu, & Gellman, 2015; Perczel, Gáspári, & Csizmadia, 2005), the secondary structure is responsible for the conformational stability of proteins. With the aim of evaluating the conformational stability of our structures, the secondary structures probability was calculated and shown in Figure 2.

Error: Reference source not found shows a marked loss of β-strand content for both G33L and G37L, if compared with 2MXU-WT and 5KK3-WT models. In detail, the β-content dramatically reduces in G33L (from 64% to 39%). The β-strand content loss is a little less severe in G37L but still considerable (from 57% to 45%). In detail, the central core (V24-S26) and C-terminal region (V36-V40) of both mutants are subjected to the biggest reduction of secondary structure. This evidence is in line with changes in fluctuations and it is probably the main factor that affects the stability of such structures.

The same trend can be shown in the mutant types of 5KK3. Destabilization of the secondary structure is noticeable in the central core of both mutants. In region V24-A30 of G33L mutant (E) the β-strand content deeply decreases from 94% to 37%. The same evidence, but less severe (from 94% to 59%) can be noticed from G37L (F). In G37L, more remarkable differences are located

around the mutated site. In particular, the region comprising residues G38, V39 and V40 almost totally loses its β-strand content. Interestingly, the G-to-L substitution at position 33 also affects the C-terminal. This result can explain the increased flexibility of that region displayed in Figure 1.
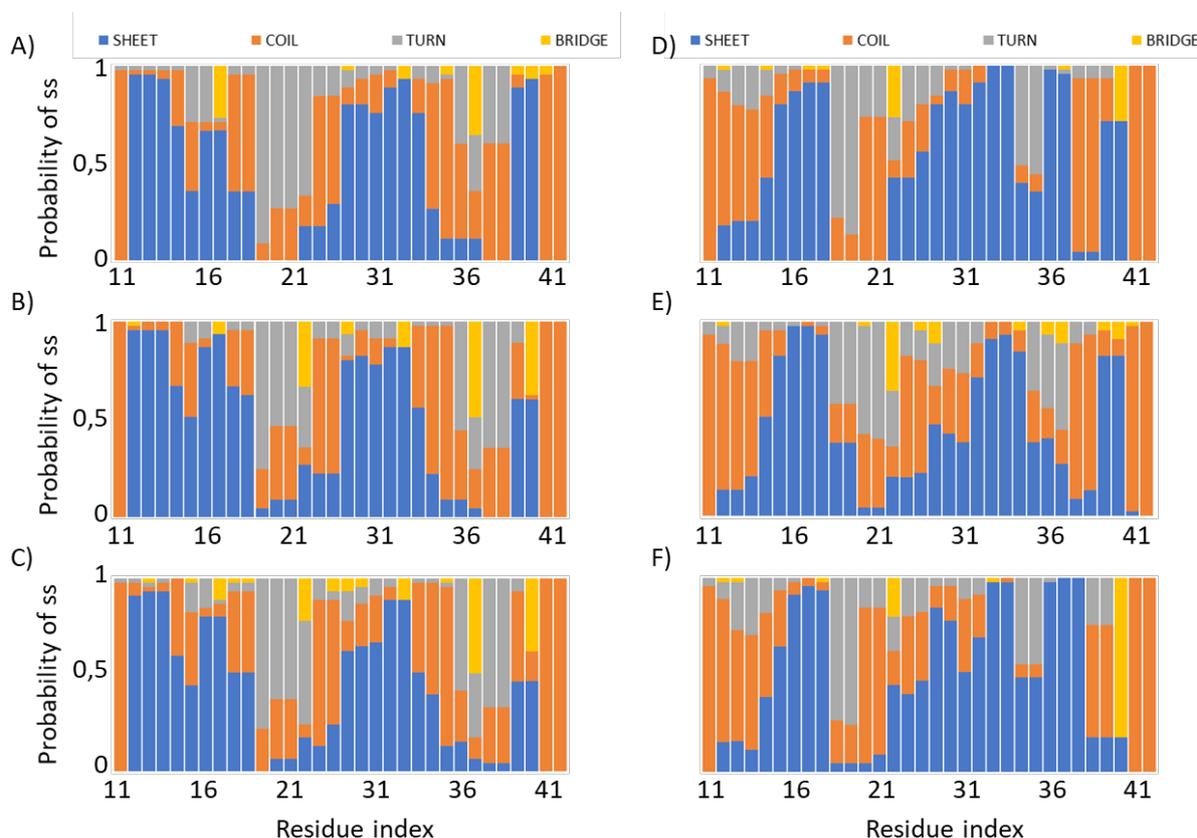

Figure 2: Probability of secondary structure averaged on the chains for the six species: A) 2MXU-WT, B) 2MXU-G33L, C) 2MXU-G37L, D) 5KK3-WT, E) 5KK3-G33L, F) 5KK3-G37L.

The total and per residue Solvent Accessible Surface Area (SASA) were calculated as a measure of the tendency of structures to reach a stable and compact arrangement. The first column of each panel in Figure 3 shows the total SASA for the two WT species and 5KK3 ($SASA[5KK3WT]=136,22\pm4,08\,nm^2$) is slightly higher than that of 2MXU ($SASA[2MXUWT]=128,34\pm3,00\,nm^2$). This result suggests that 2MXU reaches a more compact arrangement.

The hydrophobic Solvent Accessible Surface Area (blue column) slightly increases in all the mutated species. This is an expected result, considering that the glycine substitution with leucine increases the hydrophobicity(Kyte & Doolittle, 1982). The mutants also increase the total exposed surface, suggesting less stable and compact arrangements. In a greater detail, the

protein Solvent Accessible Surface Area in case of G33L mutation $\left(SASA_{2MXU}=145,06\pm4,23\,nm^2 \land SASA_{5KK3}=148,01\pm5,75\,nm^2\right)$ is higher than G37L $\left(SAS A_{2MXU}=140,55\pm1,99\,nm^2 \land SAS A_{5KK3}=136,32\pm4,93\,nm^2\right)$ and WT ($SAS A_{2MXU}=128,35\pm3,11\,nm^2 \land SAS A_{5KK3}=136,22\pm4,08\,nm^2$) in both 2MXU and 5KK3 molecular system.
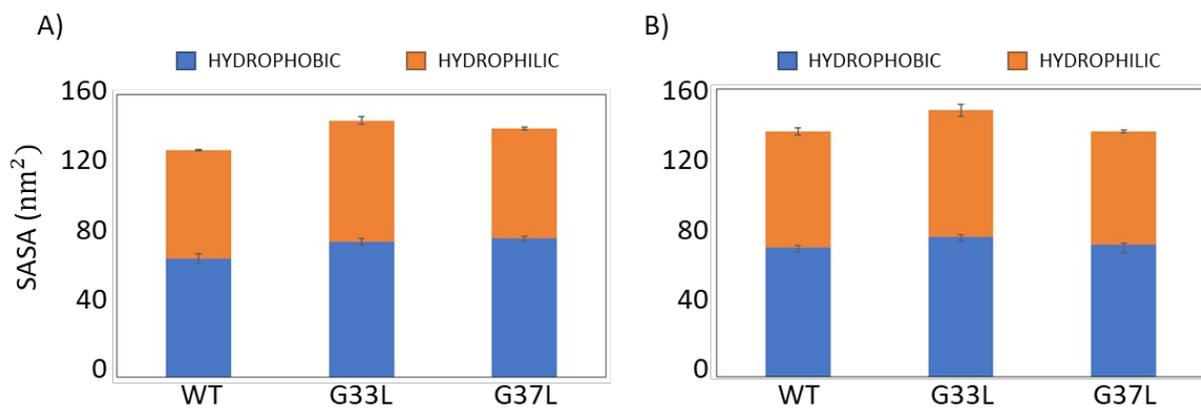

Figure 3: Total Solvent Accessible Surface Area and relative standard deviation of A) 2MXU and B) 5KK3 molecular systems. Data have been calculated as an average over the last 20 ns of each simulation.

The SASA value per residue is displayed in Error: Reference source not found. It shows a global increased tendency in the species obtained from 2MXU model (A) for exposing residues to solvent, due to the substitution, in residues E22, D23 and in the mutated site of G37L mutant. It is worth mentioning the differences in residue K28 in the 2MXU species ($SASA_{WT}=0,528\pm0,095\,nm^2, SASA_{G33L}=0,887\pm0,177\,nm^2, SASA_{G37L}=0,733\pm0,160\,nm^2$), and in the 5KK3 species ($SASA_{WT}=0,638\pm0,125\,nm^2, SASA_{G33L}=01,091\pm0,197\,nm^2, SASA_{G37L}=0,676\pm0,132\,nm^2$), since it is a key residue for stabilizing the S-shaped of Aβ_{42}(Xiao et al., 2015). These results support the changes in RMSF (Error: Reference source not found) and secondary structure (Figure 2).

The 5KK3 mutant types (B) do not show the same enhanced tendency to expose residues E22 and D23 to solvent. However, also in this case, G33L and G37L mutations affect the solvent exposure profile of the fibril. In detail, differences in residue K28 ($SAS A_{WT}=0,638\pm0,125\,nm^2$ and $SAS A_{G33L}=1,091\pm0,197\,nm^2$) and G37 ($SAS A_{WT}=0,279\pm0,057\,nm^2$ and $SAS A_{G37L}=0,696\pm0,150\,nm^2$) are worth to be mentioned.
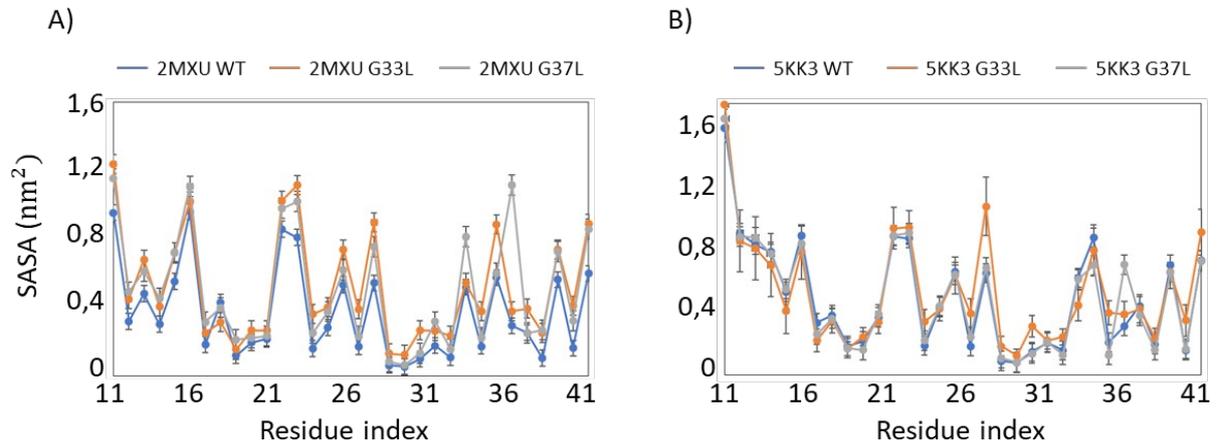
Figure 4: Solvent Accessible Surface Area per residue of wild type and G33L and G37L, in the 2MXU model (A) and in the 5KK3 model (B), calculated as an average over the last 20 ns of each simulation.

With the aim of analyzing the structural stability of the proteins, the order parameter (ordP) was calculated as reported in Material and Methods section of the manuscript. The value of the order parameter (Figure 5) emphasizes the effects of G-to-L substitutions on structural stability. In detail, the G33L mutation strongly decreases the fibril order parameter ($ord\,P_{2\,MXU-G33L}=0.7\pm0.05, \sigma_{5KK3-G33L}=0.74\pm0.04 \dot{c}$ if compared with the wild type assembly ($ord\,P_{2\,MXU}=0.91\pm0.02, \sigma_{5\,KK3}=0.9\pm0.05\dot{c}$. It is worth mentioning that the fibril stability is less affected by the G37L substitution ($ord\,P_{2\,MXU-G33L}=0.83\pm0.09, \sigma_{5\,KK3-G33L}=0.89\pm0.03\dot{c}$, in line with previous observations (Figure 1).
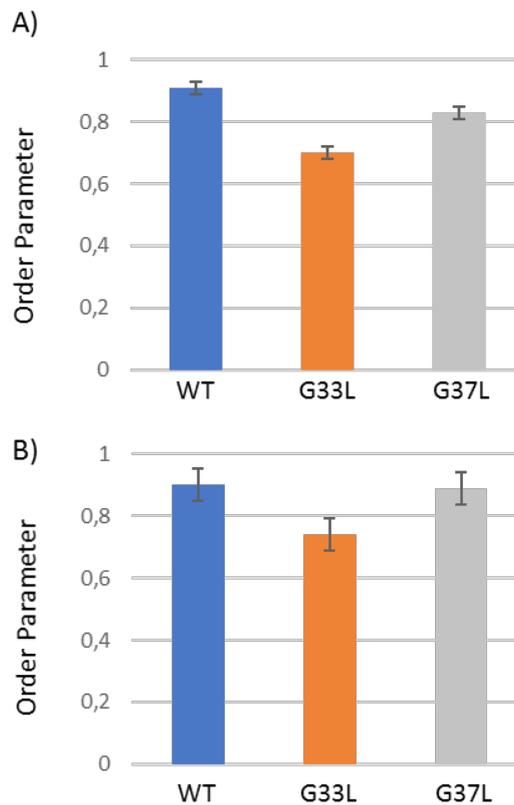
Figure 5: Expected value and corresponding standard deviation of the order parameter, calculated over the last 10 ns of each MD trajectory and averaged over the 5 replicas of each system. The panel A) shows the three species of 2MXU model, the panel B) shows the three species of 5KK3.

With the aim of highlighting the per-residue alignment along the fibril structure, the order parameter is computed as a function of the residue index (Figure 6). Overall, N-terminal tail is the most disordered region in all the six structures evaluated. The fibril's central core (residues D23-S26) and the C-terminal tail of both G33L mutant types, are subjected to a notable distortion. On the other hands, the effect of G37L substitution is less remarkable, as demonstrated by a similar order parameter along the fibril chain when compared to WT, especially in 5KK3 model. All these results are consistent with fluctuations and changes in the secondary structure (Figure 1 and Figure 2). The visual inspection of the final MD snapshots extracted from each MD replica is reported in Error: Reference source not found. As expected, the G33L mutants of both investigated polymorphisms (2MXU and 5KK3 model) are characterized by a conformational disorder, in accordance to the evidence that the disruption of the glycine zipper causes important conformational changes of the $A\beta$ assembly.
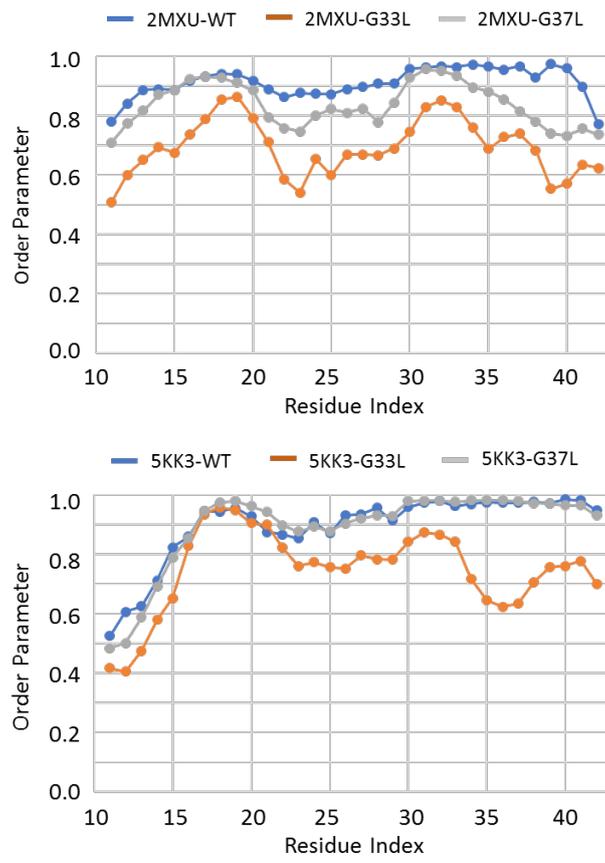
Figure 6. Order parameter as a function of the residue index in the 2MXU model (top) and 5KK3 model (bottom).
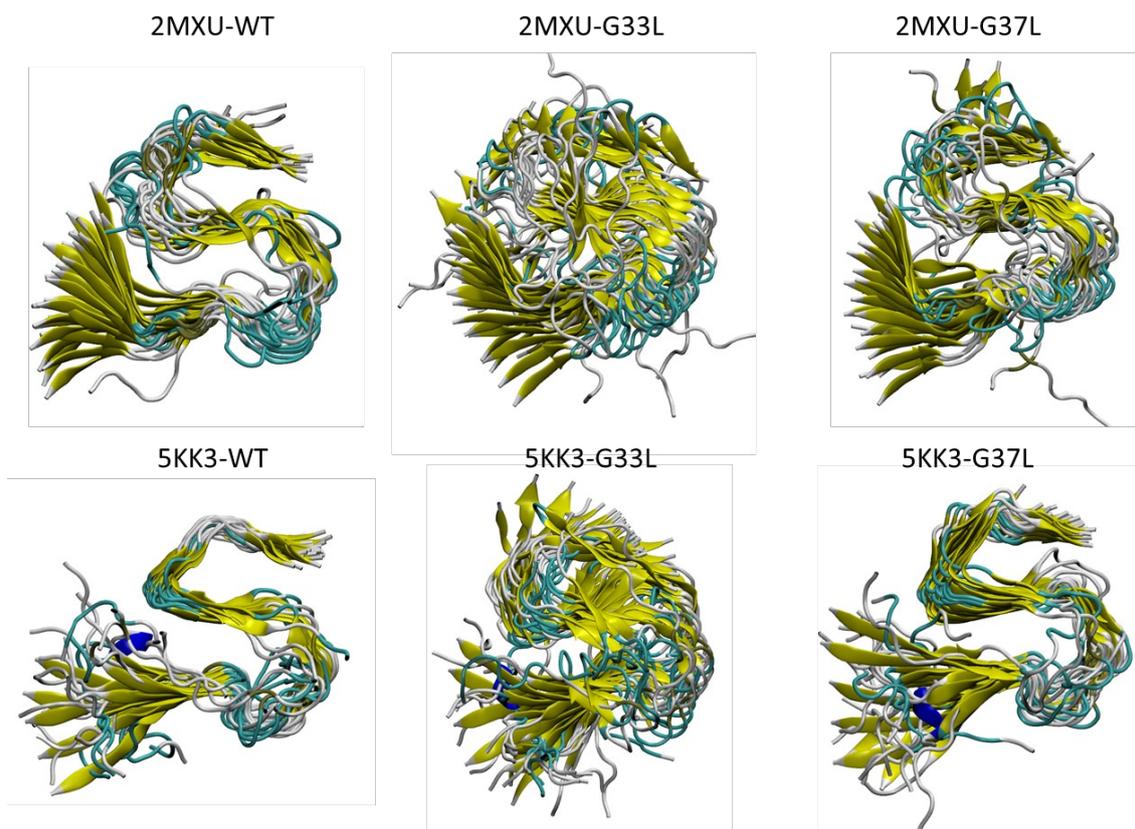
Figure 7. Visual inspection of the superimposition of snapshots taken from the end of each MD replica.

4. Discussion

Protein aggregation is implicated into a broad range of human illnesses. Alzheimer's Disease is characterized by aggregates of two types amyloid-beta peptides in the brain of patients: $A\beta_{40} \wedge A\beta_{42}$. The precise mechanisms of aggregation remain unclear, but six residues were identified to be essential for the formation of such aggregates: H14, E22, D23, G33, G37 and G38(Hsu et al., 2018). Two of the six residue proposed, G33 and G37, are involved in a GxxxG motif called glycine zipper(Kim et al., 2005). Since the GxxxG motif has a key role in the fibril formation(Harmeier et al., 2009; Liu et al., 2005; Munter et al., 2007), a detailed investigation of specific aminoacidic substitutions may help to clarify mechanisms behind aggregation and oligomerization of Aβ. In order to address this issue, two glycine-to-leucine substitutions on two different models of Aβ_{42} (2MXU and 5KK3) have been investigated: G33L and G37L. Leucine was used to replace glycine, because, unlike alanine(Russ & Engelman, 2000), LxxxG motif and GxxxL are not implicated in protein-protein interactions, and as successfully proposed by Hung et al.(Hung et al., 2008) In this scenario, this work is aimed to be complementary to the evidences proposed by Harmeier et

ai.(Harmeier et al., 2009), Hung et al.(Hung et al., 2008) and Fonte et ai.(Fonte et al., 2011).

The mutant types were seen to undergo remarkable changes in the conformational stability. These evidences substantially highlight the key role of the glycine zipper in the mechanism of fibril formation. In greater detail, the G33L mutation leads to enhanced flexibility of the central hydrophobic core of the fibril assembly, while the effect of the G37L substitution is less pronounced (Figure 1, Figure 6). The highlighted loss of structural order is in line with changes in the fibril secondary structure (Figure 2), since a marked loss of β-strand content is clearly visible in the most flexible regions. This evidence is in accordance with results shown by Perczel et al., which demonstrated that β-strands stabilize and give strength to peptides(Perczel et al., 2005).

The residue K28 has shown an increased tendency to expose itself to the solvent in both mutants of 2MXU specie and in the G33L of 5KK3 specie, as reported in Figure 4. As reported from solid-state NMR, residue K28 of S-shaped structure of $A\beta_{42}$ is involved in an intramolecular salt bridge (SB) with residue A42 that stabilizes the triple β-motif(Xiao et al., 2015). This finding suggests that the increased solvent exposure of residue K28 can lead to the disruption of K28-A42 and destabilize the structure of the folded protein(Bosshard, Marti, & Jelesarov, 2004).

Moreover, changes in the exposed hydrophobic surface (Figure 3) are substantially supported by literature because, according to the scale of Kyte and Doolittle(Kyte & Doolittle, 1982), the substitution of a glycine to a leucine increases the hydrophobicity by 0,15. The total SASA represents another significant contribution to the reduced stability of mutant types(Chien, Hwang, & Huang, 2012). The value of SASA is related to the tendency of a protein to reach a stable and compact arrangements and, in our cases decrease as follow, for both model: G33L>G37L>WT.

To summarize, our data confirm the importance of residues G33 and G37 for formation of $A\beta_{42}$ fibrils, since the substitutions here investigated notably affect the conformational dynamics and structural stability of the peptides. Our study highlights how the stability of $A\beta_{1-42}$ fibrils is a complex and delicate equilibrium between hydrophobic and hydrophilic thermodynamic forces. In particular, G33 of the central glycine zipper has been proposed to be essential for assuring

stability and promoting the process of fibril formation. It has also been proposed(Harmeier et al., 2009; Hung et al., 2008) that the aggregation of $A\beta_{42}$ is alleviated by enhancing the hydrophobicity at position G33 with G-to-A or G-to-I substitution. We also find that G37L mutant type of the 2MXU model appears less stable. These evidences, combined with the studies early mentioned(Fonte et al., 2011; Harmeier et al., 2009; Hung et al., 2008), confirm that the disruption of the glycine zipper can reduce the aggregation propensity of $A\beta_{42}$.

Additional computational studies might yield a more detailed insight into the effects of mutations in such region.

On the basis of our data, further investigations might consider this key region as a binding site for inhibitors drugs aimed at reducing the stability of the Aβ fibrils.

Conclusions

In the present paper, two different glycine-to-leucine substitutions at position 33 and 37 were analyzed and compared in two models of $A\beta_{11-42}$. Molecular Dynamics simulations in explicit solvent were performed to study their dynamic behavior in physiological environment and how mutations affect the aggregation tendency of $A\beta_{42}$. MD clearly showed that the disruption of the glycine zipper, induced by specific aminoacidic substitutions, causes conformational changes and leads to an enhanced instability of the structure. The results are in line with earlier experimental and computational studies(Fonte et al., 2011; Harmeier et al., 2009; Hung et al., 2008), indicating that binding glycine zipper might be helpful for developing new Aβ inhibitors.

References

Abraham, M. J., Murtola, T., Schulz, R., Páll, S., Smith, J. C., Hess, B., & Lindahl, E. (2015). GROMACS: High performance molecular simulations through multi-level parallelism from laptops to supercomputers. *SoftwareX*, *1–2*, 19–25. https://doi.org/10.1016/j.softx.2015.06.001

Acosta, D. M. Á. V., Vega, B. C., Basurto, J. C., Morales, L. G. F., & Rosales Hernández, M. C. (2018). Recent Advances by In Silico and In Vitro Studies of Amyloid-β 1-42 Fibril Depicted a S-Shape Conformation. *International Journal of Molecular Sciences*, *19*(8), 2415. https://doi.org/10.3390/ijms19082415

Bartus, R. T. (2000). On Neurodegenerative Diseases, Models, and Treatment Strategies: Lessons Learned and Lessons Forgotten a Generation Following the Cholinergic Hypothesis. *Experimental Neurology*, *163*(2), 495–529. https://doi.org/10.1006/exnr.2000.7397

Berendsen, H. J. C., Postma, J. P. M., Van Gunsteren, W. F., DiNola, A., & Haak, J. R. (1984). Molecular dynamics with coupling to an external bath. *The Journal of Chemical Physics*, *81*(8), 3684–3690. https://doi.org/10.1063/1.448118

Bidone, T. C., Kim, T., Deriu, M. A., Morbiducci, U., & Kamm, R. D. (2015). Multiscale impact of nucleotides and cations on the conformational equilibrium, elasticity and rheology of actin filaments and crosslinked networks. *Biomechanics and Modeling in Mechanobiology*, *14*(5), 1143–1155. https://doi.org/10.1007/s10237-015-0660-6

Bosshard, H. R., Marti, D. N., & Jelesarov, I. (2004). Protein stabilization by salt bridges: concepts, experimental approaches and clarification of some misunderstandings. *Journal of Molecular Recognition*, *17*(1), 1–16. https://doi.org/10.1002/jmr.657

Bussi, G., Donadio, D., & Parrinello, M. (2007). Canonical sampling through velocity rescaling. *Journal of Chemical Physics*, *126*(1), 014101. https://doi.org/10.1063/1.2408420

Chien, Y.-T., Hwang, J.-K., & Huang, S.-W. (2012). On the Relationship Between Residue Solvent Exposure and Thermal Fluctuations in Proteins. In *Protein Structure*. InTech. https://doi.org/10.5772/37148

Chiti, F., Stefani, M., Taddei, N., Ramponi, G., & Dobson, C. M. (2003). Rationalization of the effects of mutations on peptide andprotein aggregation rates. *Nature*, *424*(6950), 805–808. https://doi.org/10.1038/nature01891

Colvin, M. T., Silvers, R., Ni, Q. Z., Can, T. V., Sergeyev, I., Rosay, M., … Griffin, R. G. (2016a). Atomic Resolution Structure of Monomorphic Aβ $_{42}$ Amyloid Fibrils. *Journal of the American Chemical Society*, *138*(30), 9663–9674. https://doi.org/10.1021/jacs.6b05129

Colvin, M. T., Silvers, R., Ni, Q. Z., Can, T. V, Sergeyev, I., Rosay, M., … Griffin, R. G. (2016b). Atomic Resolution Structure of Monomorphic Aβ42 Amyloid Fibrils. *Journal of the American Chemical Society*, *138*(30), 9663–9674. https://doi.org/10.1021/jacs.6b05129

Cummings, J. L. (2004). Alzheimer's Disease. *New England Journal of Medicine*, *351*(1), 56–67. https://doi.org/10.1056/NEJMra040223

Darden, T., York, D., & Pedersen, L. (1993). Particle mesh Ewald: An N·log(N) method for Ewald sums in large systems. *The Journal of Chemical Physics*, *98*(12), 10089. https://doi.org/10.1063/1.464397

Deriu, M. A. M. A., Grasso, G., Tuszynski, J. A. J. A., Massai, D., Gallo, D., Morbiducci, U., & Danani, A. (2016). Characterization of the AXH domain of Ataxin-1 using enhanced sampling and functional mode analysis. *Proteins: Structure, Function, and Bioinformatics*, *84*(5), 666–673. https://doi.org/10.1002/prot.25017

Evans, D. J., & Holian, B. L. (1985). The Nose–Hoover thermostat. *The Journal of Chemical Physics*, *83*(8), 4069–4074. https://doi.org/10.1063/1.449071

Fändrich, M., Meinhardt, J., & Grigorieff, N. (n.d.). Structural polymorphism of Alzheimer Abeta and other amyloid fibrils. *Prion*, *3*(2), 89–93.

Fletcher, R., & Powell, M. J. D. (1963). A Rapidly Convergent Descent Method for Minimization. *The Computer Journal*, *6*(2), 163–168. https://doi.org/10.1093/comjnl/6.2.163

Fonte, V., Dostal, V., Roberts, C. M., Gonzales, P., Lacor, P., Magrane, J., … Link, C. D. (2011). A glycine zipper motif mediates the formation of toxic β-amyloid oligomers in vitro and in vivo. *Molecular Neurodegeneration*, *6*(1), 61. https://doi.org/10.1186/1750-1326-6-61

Grasso, G, Morbiducci, U., Massai, D., Tuszynki, J., Danani, A., & Deriu, M. (2018). Destabilizing the AXH Tetramer by Mutations: Mechanisms and Potential Antiaggregation Strategies. *Biophysical Journal*, *114*(2), 323–330. https://doi.org/10.1016/j.bpj.2017.11.025

Grasso, Gianvito, Rebella, M., Morbiducci, U., Tuszynski, J. A., Danani, A., & Deriu, M. A. (2019). The Role of Structural Polymorphism in Driving the Mechanical Performance of the Alzheimer's Beta Amyloid Fibrils. *Frontiers in Bioengineering and Biotechnology*, *7*, 83. https://doi.org/10.3389/fbioe.2019.00083

Grasso, Gianvito, Rebella, M., Muscat, S., Morbiducci, U., Tuszynski, J., Danani, A., & Deriu, M. (2018). Conformational Dynamics and Stability of U-Shaped and S-Shaped Amyloid β Assemblies. *International Journal of Molecular Sciences*, *19*(2), 571. https://doi.org/10.3390/ijms19020571

Gravina, S. A., Ho, L., Eckman, C. B., Long, K. E., Otvos, L., Younkin, L. H., … Younkin, S. G. (1995). Amyloid beta protein (A beta) in Alzheimer's disease brain. Biochemical and immunocytochemical analysis with antibodies specific for forms ending at A beta 40 or A beta 42(43). *The Journal of Biological Chemistry*, *270*(13), 7013–7016. https://doi.org/10.1074/JBC.270.13.7013

Hardy, J., & Selkoe, D. J. (2002). The amyloid hypothesis of Alzheimer's disease: progress and problems on the road to therapeutics. *Science (New York, N.Y.)*, *297*(5580), 353–356. https://doi.org/10.1126/science.1072994

Harmeier, A., Wozny, C., Rost, B. R., Munter, L.-M., Hua, H., Georgiev, O., … Multhaup, G. (2009). Role of amyloid-beta glycine 33 in oligomerization, toxicity, and neuronal plasticity. *The Journal of Neuroscience : The Official Journal of the Society for Neuroscience*, *29*(23), 7582–7590. https://doi.org/10.1523/JNEUROSCI.1336-09.2009

Heinig, M., & Frishman, D. (2004). STRIDE: a web server for secondary structure assignment from known atomic coordinates of proteins. *Nucleic Acids Research*, *32*(Web Server issue), W500–W502. https://doi.org/10.1093/nar/gkh429

Hess, B., Bekker, H., Berendsen, H. J. C., & Fraaije, J. G. E. M. (1997). LINCS: A linear constraint solver for molecular simulations. *Journal of Computational Chemistry*, *18*(12), 1463–1472. https://doi.org/10.1002/(SICI)1096-987X(199709)18:12<1463::AID-JCC4>3.0.CO;2-H

Hsu, F., Park, G., & Guo, Z. (2018). Key Residues for the Formation of Aβ42 Amyloid Fibrils. *ACS Omega*, *3*(7), 8401–8407. https://doi.org/10.1021/acsomega.8b00887

Huang, J., Rauscher, S., Nawrocki, G., Ran, T., Feig, M., De Groot, B. L., … MacKerell, A. D. (2016). CHARMM36m: An improved force field for folded and intrinsically disordered proteins. *Nature Methods*, *14*(1), 71–73. https://doi.org/10.1038/nmeth.4067

Huet, A., & Derreumaux, P. (2006). Impact of the Mutation A21G (Flemish Variant) on Alzheimer's β-Amyloid Dimers by Molecular Dynamics Simulations. *Biophysical Journal*, *91*(10), 3829–3840. https://doi.org/10.1529/biophysj.106.090993

Humphrey, W., Dalke, A., & Schulten, K. (1996). VMD: visual molecular dynamics. *Journal of Molecular Graphics*, *14*(1), 33–38, 27–28. https://doi.org/10.1016/0263-7855(96)00018-5

Hung, L. W., Ciccotosto, G. D., Giannakis, E., Tew, D. J., Perez, K., Masters, C. L., … Barnham, K. J. (2008). Amyloid-beta peptide (Abeta) neurotoxicity is modulated by the rate of peptide aggregation: Abeta dimers and trimers correlate with neurotoxicity. *The Journal of Neuroscience : The Official Journal of the Society for Neuroscience*, *28*(46), 11950–11958. https://doi.org/10.1523/JNEUROSCI.3916-08.2008

Jorgensen, W. L., Chandrasekhar, J., Madura, J. D., Impey, R. W., & Klein, M. L. (1983). Comparison of simple potential functions for simulating liquid water. *The Journal of Chemical Physics*, *79*(2), 926–935. https://doi.org/10.1063/1.445869

Kim, S., Jeon, T.-J., Oberai, A., Yang, D., Schmidt, J. J., & Bowie, J. U. (2005). Transmembrane glycine zippers: physiological and pathological roles in membrane proteins. *Proceedings of the National Academy of Sciences of the United States of America*, *102*(40), 14278–14283. https://doi.org/10.1073/pnas.0501234102

Kung, V. M., Cornilescu, G., & Gellman, S. H. (2015). Impact of Strand Number on Parallel β-Sheet Stability. *Angewandte Chemie (International Ed. in English)*, *54*(48), 14336–14339. https://doi.org/10.1002/anie.201506448

Kyte, J., & Doolittle, R. F. (1982). A simple method for displaying the hydropathic character of a protein. *Journal of Molecular Biology*, *157*(1), 105–132. https://doi.org/10.1016/0022-2836(82)90515-0

Lee, H. J., Korshavn, K. J., Nam, Y., Kang, J., Paul, T. J., Kerr, R. A., … Lim, M. H. (2017). Structural and Mechanistic Insights into Development of Chemical Tools to Control Individual and Inter-Related Pathological Features in Alzheimer's Disease. *Chemistry (Weinheim an Der Bergstrasse, Germany)*, *23*(11), 2706–2715. https://doi.org/10.1002/chem.201605401

Liu, W., Crocker, E., Zhang, W., Elliott, J. I., Luy, B., Li, H., … Smith, S. O. (2005). Structural Role of Glycine in Amyloid Fibrils Formed from Transmembrane α-Helices [†]. *Biochemistry*, *44*(9), 3591–3597. https://doi.org/10.1021/bi047827g

Lu, J.-X., Qiang, W., Yau, W.-M., Schwieters, C. D., Meredith, S. C., & Tycko, R. (2013). Molecular structure of β-amyloid fibrils in Alzheimer's disease brain tissue. *Cell*, *154*(6), 1257–1268. https://doi.org/10.1016/j.cell.2013.08.035

Lührs, T., Ritter, C., Adrian, M., Riek-Loher, D., Bohrmann, B., Döbeli, H., … Riek, R. (2005). 3D structure of Alzheimer's amyloid-beta(1-42) fibrils. *Proceedings of the National Academy of Sciences of the United States of America*, *102*(48), 17342–17347. https://doi.org/10.1073/pnas.0506723102

Munter, L.-M., Voigt, P., Harmeier, A., Kaden, D., Gottschalk, K. E., Weise, C., … Multhaup, G. (2007). GxxxG motifs within the amyloid precursor protein transmembrane sequence are critical for the etiology of Abeta42. *The EMBO Journal*, *26*(6), 1702–1712. https://doi.org/10.1038/sj.emboj.7601616

Ngo, S. T., Nguyen, M. T., Nguyen, N. T., & Vu, V. V. (2017). The Effects of A21G Mutation on Transmembrane Amyloid Beta (11–40) Trimer: An *In Silico* Study. *The Journal of Physical Chemistry B*, *121*(36), 8467–8474. https://doi.org/10.1021/acs.jpcb.7b05906

Paravastu, A. K., Leapman, R. D., Yau, W.-M., & Tycko, R. (2008). Molecular structural basis for polymorphism in Alzheimer's beta-amyloid fibrils. *Proceedings of the National Academy of Sciences of the United States of America*, *105*(47), 18349–18354. https://doi.org/10.1073/pnas.0806270105

Perczel, A., Gáspári, Z., & Csizmadia, I. G. (2005). Structure and stability of β-pleated sheets. *Journal of Computational Chemistry*, *26*(11), 1155–1168. https://doi.org/10.1002/jcc.20255

Petkova, A. T., Ishii, Y., Balbach, J. J., Antzutkin, O. N., Leapman, R. D., Delaglio, F., & Tycko, R. (2002). A structural model for Alzheimer's -amyloid fibrils based on experimental constraints from solid state NMR. *Proceedings of the National Academy of Sciences*, *99*(26), 16742–16747. https://doi.org/10.1073/pnas.262663499

Pettersen, E. F., Goddard, T. D., Huang, C. C., Couch, G. S., Greenblatt, D. M., Meng, E. C., & Ferrin, T. E. (2004). UCSF Chimera?A visualization system for exploratory research and analysis. *Journal of Computational Chemistry*, *25*(13), 1605–1612. https://doi.org/10.1002/jcc.20084

Qiang, W., Yau, W.-M., Luo, Y., Mattson, M. P., & Tycko, R. (2012). Antiparallel β-sheet architecture in Iowa-mutant β-amyloid fibrils. *Proceedings of the National Academy of Sciences of the United States of America*, *109*(12), 4443–4448. https://doi.org/10.1073/pnas.1111305109

Querfurth, H. W., & LaFerla, F. M. (2010). Alzheimer's Disease. *The New England Journal of Medicine*, *362*(4), 329–344. https://doi.org/10.1056/NEJMra0909142

Roher, A. E., Lowenson, J. D., Clarke, S., Woods, A. S., Cotter, R. J., Gowing, E., & Ball, M. J. (1993). beta-Amyloid-(1-42) is a major component of cerebrovascular amyloid deposits: implications for the pathology of Alzheimer disease. *Proceedings of the National Academy of Sciences of the United States of America*, *90*(22), 10836–10840. https://doi.org/10.1073/PNAS.90.22.10836

Russ, W. P., & Engelman, D. M. (2000). The GxxxG motif: A framework for transmembrane helix-helix association. *Journal of Molecular Biology*, *296*(3), 911–919. https://doi.org/10.1006/jmbi.1999.3489

Sato, T., Kienlen-Campard, P., Ahmed, M., Liu, W., Li, H., Elliott, J. I., … Smith, S. O. (2006). Inhibitors of Amyloid Toxicity Based on β-sheet Packing of Aβ40 and Aβ42[†]. *Biochemistry*, *45*(17), 5503–5516. https://doi.org/10.1021/bi052485f

Schütz, A. K., Vagt, T., Huber, M., Ovchinnikova, O. Y., Cadalbert, R., Wall, J., … Meier, B. H. (2015). Atomic-Resolution Three-Dimensional Structure of Amyloid β Fibrils Bearing the Osaka Mutation. *Angewandte Chemie International Edition*, *54*(1), 331–335. https://doi.org/10.1002/anie.201408598

Selkoe, D. J., & Hardy, J. (2016). The amyloid hypothesis of Alzheimer's disease at 25 years. *EMBO Molecular Medicine*, *8*(6), 595–608. https://doi.org/10.15252/emmm.201606210

Soncini, M., Vesentini, S., Ruffoni, D., Orsi, M., Deriu, M. A., & Redaelli, A. (2007). Mechanical response and conformational changes of alpha-actinin domains during unfolding: A molecular dynamics study. *Biomechanics and Modeling in Mechanobiology*, *6*(6), 399–407. https://doi.org/10.1007/s10237-006-0060-z

Wälti, M. A., Ravotti, F., Arai, H., Glabe, C. G., Wall, J. S., Böckmann, A., … Riek, R. (2016). Atomic-resolution structure of a disease-relevant Aβ(1-42) amyloid fibril. *Proceedings of the National Academy of Sciences of the United States of America*, *113*(34), E4976-84. https://doi.org/10.1073/pnas.1600749113

Xi, W., Wang, W., Abbott, G., & Hansmann, U. H. E. (2016). Stability of a Recently Found Triple-β-Stranded Aβ1–42 Fibril Motif. *The Journal of Physical Chemistry B*, *120*(20), 4548–4557. https://doi.org/10.1021/acs.jpcb.6b01724

Xiao, Y., Ma, B., McElheny, D., Parthasarathy, S., Long, F., Hoshi, M., … Ishii, Y. (2015). Aβ(1–42) fibril structure illuminates self-recognition and replication of amyloid in Alzheimer's disease. *Nature Structural & Molecular Biology*, *22*(6), 499–505. https://doi.org/10.1038/nsmb.2991

Acknowledgement

Author Contributions

GG, and MAD conceived the research.

GG, and LL did the molecular dynamics simulations.

GG, LL and MAD analyzed and rationalized the data.

All authors wrote the paper and critically commented to the manuscript.

All authors read and approved the final manuscript.

Competing Interests

The authors declare no competing interests